THE JOURNAL OF PHYSICAL CHEMISTRY Letters

Letter

pubs.acs.org/JPCL

Toward Quantitative Measurements of Enzyme Kinetics by Dissolution Dynamic Nuclear Polarization

Emeric Miclet,[†,‡,§] Daniel Abergel,*[,†,‡,§] Aurélien Bornet,[∥] Jonas Milani,[∥] Sami Jannin,[†,‡,§,∥,⊥] and Geoffrey Bodenhausen[†,‡,§,∥]

[†]École Normale Supérieure-PSL Research University, Département de Chimie, 24 rue Lhomond, F-75005 Paris, France

[‡]Sorbonne Universités, UPMC Univ Paris 06, LBM, 4 place Jussieu, F-75005, Paris, France

[§]CNRS, UMR 7203 LBM, F-75005, Paris, France

[∥]Institut des Sciences et Ingénierie Chimiques, Ecole Polytechnique Fédérale de Lausanne (EPFL), Batochime, CH-1015 Lausanne, Switzerland

[⊥]Bruker BioSpin AG, Industriestrasse 26, 8117 Fällanden, Switzerland

ABSTRACT: Dissolution dynamic nuclear polarization (D-DNP) experiments enabled us to study the kinetics of the enzymatic phosphorylation reaction of glucose to form glucose-6-phosphate (G6P) by hexokinase (HK), with or without the presence of an excess of G6P, which is known to be an inhibitor of the enzyme. Against all expectations, our observations demonstrate that the phosphorylation of both α and β glucose anomers occurs with comparable kinetics. The catalytic constant of the reaction was estimated based on a simple kinetic model tailored for hyperpolarized systems.

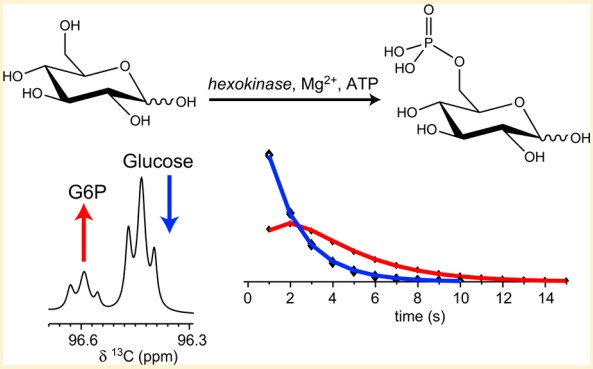

SECTION: Biophysical Chemistry and Biomolecules

NMR spectroscopy and imaging of low abundant substrates have benefitted from advances of hyperpolarization techniques aiming at the enhancement of nuclear spin polarizations well beyond Boltzmann equilibrium. Among these hyperpolarization techniques, dissolution dynamic nuclear polarization (D-DNP)[1,2] has proven to be very efficient for boosting the nuclear spin polarization of a broad variety of small ^{13}C-labeled molecules in solution. The sensitivity of NMR or MRI is directly proportional to the nuclear spin polarization, which can be enhanced by up to 4 or 5 orders of magnitude. Many applications have emerged thanks to the improved sensitivity, ranging from the detection of reaction intermediates[3,4] to the real-time metabolic imaging of tumors in vivo[5] and the detection of their response to medical treatment.[6]

Several groups have recently demonstrated the possibility of monitoring metabolic processes in vitro, in cell suspensions or living tissues. To date, only a limited number of D-DNP NMR studies have focused on the in vitro investigation of protein−substrate interactions[7] or enzyme kinetics.[8,9] These studies open new avenues for the investigation of fast kinetic processes, on time scales of seconds rather than minutes, as is customarily achieved by conventional ^{1}H and ^{13}C NMR. On longer time scales, the degradation or rearrangements of substrates or products may skew quantitative measurements. By contrast, the sensitivity gains provided by D-DNP allow one to perform experiments in such a short time that the spontaneous evolution of the metabolites during the measurement process is limited, which therefore appears to offer a more accurate way of investigating enzyme kinetics.

Glucose is a substrate of paramount importance for living cells and organisms. It is involved in glycolysis and serves as the precursor of the pentose phosphate pathway (PPP). The metabolism of glucose can be altered under various pathological circumstances. Hyperpolarization by dissolution-DNP may provide a way to witness such alterations, as was recently shown for cancer cell cultures.[10] In this context, kinetic studies of individual enzymes contributing to the metabolism of glucose are obviously of crucial interest for detailed investigations of metabolic chains.

The main goal of this work is to characterize the phosphorylation kinetics of glucose by hexokinase (HK) on a time scale that is sufficiently short, on the order of 20 s, to prevent any interconversion of the α and β anomers of both glucose and glucose-6-phosphate (G6P). The phosphorylation of glucose represents the initial enzymatic transformation that is common to both glycolysis and PPP. This reaction consumes

Received: July 7, 2014
Accepted: September 3, 2014
Published: September 3, 2014

   dx.doi.org/10.1021/jz501411d | J. Phys. Chem. Lett. 2014, 5, 3290−3295

one molecule of adenosine triphosphate (ATP) and requires the presence of magnesium ions Mg^{2+} (Figure 1).

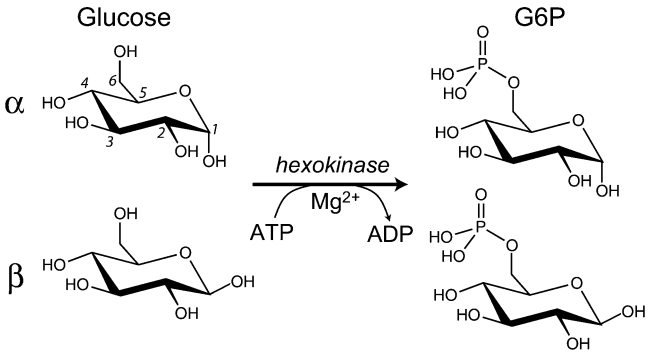

Figure 1. Phosphorylation of the α and β anomers of glucose by hexokinase. Both α and β anomers, and the numbering of the carbon atoms, are indicated.

In this Letter, we report the real time monitoring of the decrease in concentration of glucose, as it is consumed by the enzymatic reaction, and of the concomitant buildup of the G6P concentration. Our analysis of the experiments assumes a pseudo-first order reaction, justified by the presence of a large excess of ATP, and takes into account the known inhibition of hexokinase by G6P. The kinetic rate constants of the reactions can be determined thanks to a dramatic sensitivity enhancement of uniformly ^{13}C- and ^{2}H-labeled glucose afforded by D-DNP.

DNP was performed on 50 μL frozen pellets containing 5.6 M uniformly ^{13}C-enriched and deuterated glucose and 50 mM TEMPOL. After rapid dissolution (ca. 4 s), the hyperpolarized substrate was injected into an NMR tube filled with a solution of hexokinase containing Mg^{2+} and an excess of ATP (see Experimental Methods). Experiments were performed either in the absence or presence of 30 mM G6P, the reaction product that is known to act as an inhibitor of the enzyme. In each case, ^{13}C NMR spectra were acquired every second with 10° radio frequency (rf) pulses. The spectra exhibited stable frequencies and line shapes in the course of the experiments, except for signals acquired less than 2 s after injection, when the mixing of the polarized substrate with the solution is not yet completed. These signals were discarded from further analyses. The kinetics of the reaction was monitored by integrating the $^{13}C^1$ signals of both α and β anomers, because of their characteristic resonance frequencies. The $^{13}C^1$ multiplets of both α and β anomers were clearly separated and feature large $^{1}J(C^1, C^2)$ couplings in the pyranose rings. In addition, due to characteristic long-range $^{2}J(C^1, C^i)$ and $^{3}J(C^1, C^j)$ couplings,[11] the multiplets of the α and β anomers exhibit fine structures ($d \times d \times d$ and $d \times t$, respectively; see Figure 2.)

The $^{13}C^1$ resonances of G6P are slightly displaced toward higher frequencies with respect to their glucose counterparts (Figure 3). This causes partial overlaps, so that deconvolution and numerical integration of the fitted line shapes were needed to determine peak intensities. Line fitting was achieved with 12 Lorentzians for the β anomers, and 16 components for the α anomers.

Phosphorylation of glucose was studied in the presence of 250 mM ATP and 30 μM hexokinase, which corresponds to ca. 400 U of enzymatic activity. The activity was chosen so that the reaction was completed in about 5 times $T_1(^{13}C)$. Signals of

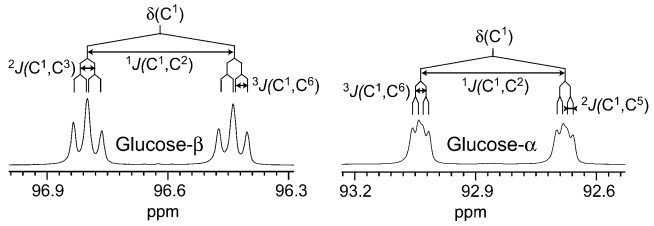

Figure 2. Details of the $^{13}C^1$ multiplets of the α and β anomers of glucose. Both halves of the C^1 multiplet arising from the large $^{1}J(C^1,C^2)$ coupling constants of the β-anomer (left) have a 1:2:1 intensity pattern, due to the nearly degenerate $^{2}J(C^1,C^3)$ and $^{3}J(C^1,C^6)$ couplings. The two halves of the $^{13}C^1$ multiplet of the α-anomer (right) appear as doublets-of-doublets with a 1:1:1:1 intensity pattern, due to the nondegenerate coupling constants $^{2}J(C^1,C^5)$ and $^{3}J(C^1,C^6)$.[10]

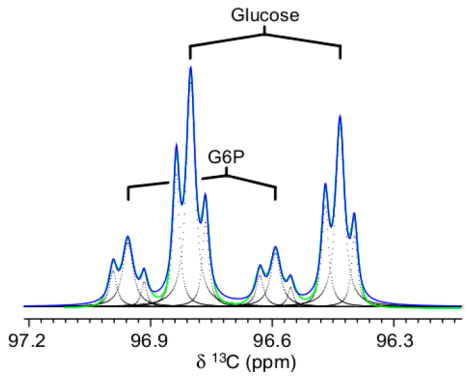

Figure 3. Interleaved multiplets of the $^{13}C^1$ resonances of the β-anomers of glucose and glucose-6-phosphate (G6P). Dotted lines indicate the optimal Lorentzian lines used to fit the various components of the spectrum. Experimental and fitted spectra are depicted in blue and green. The slight asymmetry between the two halves of each multiplet is due to a violation of the high-temperature approximation that results from DNP.

glucose and G6P could be observed for ca. 12 and 18 s, respectively (see Figure 4).

Similar decay curves of the glucose signals and G6P buildup curves were obtained for both α and β anomers, showing that both glucose anomers are phosphorylated.

This is particularly interesting, as saturation transfer difference (STD) experiments seemed to indicate that the yeast Hexokinase PII yielded predominantly α-G6P, and that α-glucose was the preferred substrate.[12] Although these studies were performed under somewhat different experimental conditions, they are in sharp contrast with the present observations that unambiguously demonstrate the production of both α- and β-G6P with comparable kinetics, starting from a solution containing both α- and β-glucose anomers in equilibrium.

Figures 4 and 5 clearly show the inhibiting effect of G6P. When G6P is initially present in the solution, the glucose and G6P signals decay almost in parallel at long times, attesting a strong enzyme inhibition. This is in contrast with the much faster decay of the glucose signals with respect to G6P in the absence of inhibitor at the beginning of the reaction.

In the presence of a large excess of ATP, and at a high HK concentrations, the reaction can be described as pseudo first-order, so that the concentrations of glucose and G6P obey the following equations:

dx.doi.org/10.1021/jz501411d | J. Phys. Chem. Lett. 2014, 5, 3290−3295

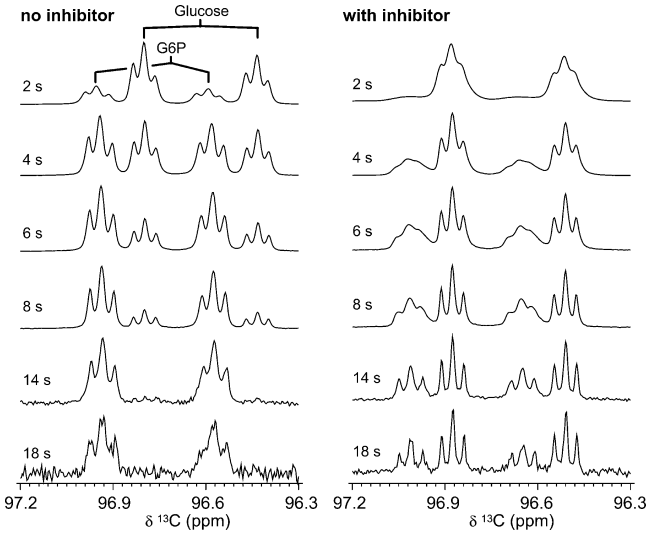

Figure 4. Time-dependent hyperpolarized $^{13}C^1$ signals of the β-anomers of glucose and G6P during phosphorylation by hexokinase. Left and right panels correspond to the evolution without and with the presence of 30 mM G6P that acts as inhibitor at the beginning of the reaction.

$$\frac{d[G]}{dt} = -k[G] \tag{1}$$

$$\frac{d[G6P]}{dt} = \frac{-d[G]}{dt} \tag{2}$$

Thus, the glucose signal intensity of the nth free induction decay is

$$S_G(n\Delta t) \sim S_0 \sin\alpha(\cos\alpha)^n[G]_0 \exp\{-(k + 1/T_1^G)n\Delta t\} \tag{3}$$

where Δt is the delay between two consecutive signal acquisitions, S_0 and $[G]_0$ are the initial glucose signal intensity and concentration, α is the flip angle of the rf pulse, and T_1^G the longitudinal relaxation time of the anomeric $^{13}C^1$ nuclei in glucose. The intensity of the G6P signals is described by[13]

$$S_{G6P} \propto (\cos\alpha)^n \int_0^{n\Delta t} \frac{d[G6P]}{d\tau} e^{-\tau/T_1^G} e^{-(n\Delta t-\tau)/T_1^{G6P}} d\tau \tag{4}$$

where T_1^{G6P} is the longitudinal relaxation time of the anomeric $^{13}C^1$ nuclei in G6P.

However, such a simple model does not account for the known fact that the reaction product G6P is an inhibitor of hexokinase. One therefore expects that the apparent kinetic rate constant k_{app} should vary in the course of the reaction, since it is proportional to the concentration [HK] of available enzyme:

$$k_{app} = k[HK] \tag{5}$$

where k is the "true" catalytic constant of the reaction. The concentration [HK] depends on the equilibrium dissociation constant K_D of the complex HK-G6P:

$$K_D = [G6P][HK]/[HK\text{-}G6P] \tag{6}$$

The total concentration $[G6P]_t$ can be expressed in terms of the following quantities: (i) [G6P] of the free reaction product, (ii) [HK-G6P] of its complex with the enzyme, (iii) $[G6P]_r$ produced by phosphorylation, and (iv) the initial concentration $[G6P]_0$ of inhibitor. These fulfill the equation:

$$[G6P]_t = [G6P] + [HK\text{-}G6P] = [G6P]_0 + [G6P]_r \tag{7}$$

One obtains:

$$K_d = \frac{[G6P][HK]}{[HK\text{-}G6P]} = \frac{([G6P]_0 + [G6P]_r - [HK\text{-}G6P])([HK]_0 - [HK\text{-}G6P])}{[HK\text{-}G6P]} \tag{8}$$

so that the concentration [HK-G6P] of the HK-G6P complex is given by the smaller root of

$$[HK\text{-}G6P]^2 - (K_d + [G6P]_0 + [G6P]_r + [HK]_0)[HK\text{-}G6P] + [HK]_0([G6P]_0 + [G6P]_r) = 0 \tag{9}$$

Combining eqs 1, 2, 5, and 6 therefore allows one to compute [G] and [G6P].

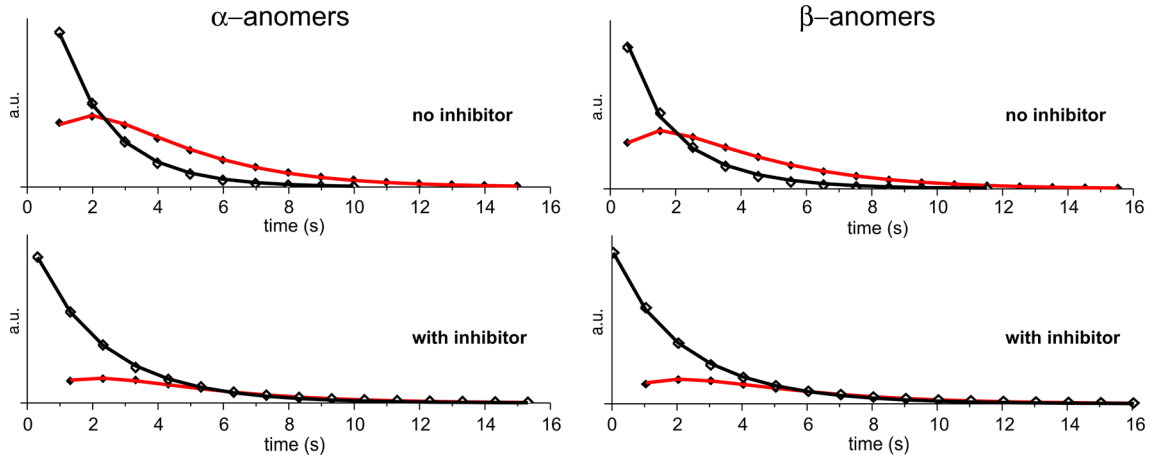

Figure 5. Integrated intensities of the experimental (symbols) and fitted (solid lines) $^{13}C^1$ multiplets of the α-anomers (left) and the β-anomers (right). Top: without inhibitor; bottom: with 30 mM inihibitor (G6P) initially present in the solution. Filled and open symbols refer to the intensities of the hyperpolarized G6P and glucose signals. The time axes are shifted by t_0, which accounts for the delayed onset of the enzymatic reaction (see Table 1 and text for details).

dx.doi.org/10.1021/jz501411d | J. Phys. Chem. Lett. 2014, 5, 3290−3295

The decay of the glucose signals and the G6P buildup curves obtained from experiments performed (A) without and (B) with G6P initially present in the buffer were analyzed simultaneously. For each anomeric $^{13}C^1$ resonance, the sums of the intensities of the high- and low-frequency submultiplets were fitted to the above equations (see Table 1). This implies

Table 1. Estimated Parameters of the Kinetic Model Obtained from Experiments A and B at 300 K (See Text for Details)

	α	β
K_D (mM)	35.0	22.5
k (s^{-1} M^{-1})	11613	18453
T_1^G (s)	3.51	3.91
T_1^{G6P} (s)	2.55	2.83
$[G]_0$ in A (mM)	8.4	26.9
$[G]_0$ in B (mM)	50.8	100
t_0 in A (s)	0.9	1.2
t_0 in B (s)	1.60	1.96

no less than 10 adjustable parameters, which may seem quite a large number. Our kinetic model forbids the use of fitting strategies relying on derivatives, since the fitting procedure tends to get trapped in local minima. In order to avoid these difficulties and to reach the global minimum, a differential evolution algorithm[14] was used to extract optimal parameters for the analysis of the $^{13}C^1$ resonances of the α and β anomers.

Note that monoexponential decays of the $^{13}C^1$ signals are expected if one neglects cross-correlated dipole−dipole and CSA mechanisms involving the $^{13}C^1$ and $^{13}C^2$ nuclei.[15] Additionally, it was observed that the $^{13}C^1$ signals of the two anomeric α and β forms have distinct values $T_1^{G\alpha}$, $T_1^{G\beta}$, $T_1^{G6P\alpha}$ and $T_1^{G6P\beta}$, which is not surprising *per se*. Results are depicted in Figure 5.

The use of a model in which the kinetic constants depend explicitly on the enzyme concentration was motivated, as mentioned above, by the known inhibiting effect of G6P on hexokinase. The introduction of this information was readily supported by the observation that the time-dependences of the glucose and G6P signals were clearly different when the experiments were performed in the presence or absence of G6P at the outset of the reaction (see Figure 5). This motivated our strategy to begin by assuming a model that encompasses the salient features of the kinetics and at the same time provides a reasonable trade-off between accuracy and complexity.

Some of the quantities appearing in the equations can be considered as known, while others must be assumed to be adjustable parameters. Thus, the total concentration of the enzyme, [HK] + [HK-G6P], as well as the initial concentration $[G6P]_0$, are well-controlled quantities, since these constituents were added to the buffer before the injection of the hyperpolarized glucose solution. On the other hand, the catalytic rate constants k, the dissociation constants K_D of the HK-G6P complex, the relaxation times T_1^G and T_1^{G6P} of the anomeric $^{13}C^1$ carbons in glucose and G6P, as well as the initial concentrations of glucose $[G]_0$ were treated as adjustable parameters. It is important to note that the values of the longitudinal T_1^G relaxation times of the ^{13}C nuclei in the α and β anomers (Table 1) were within 10% of the values extracted from a D-DNP experiment performed on pure glucose in the absence of hexokinase.

Estimating the experimental errors is difficult in the case at hand. Indeed, the signal intensities being dramatically boosted by hyperpolarization, the usual statistical tools of data analysis do not seem to be relevant, so that the confidence criteria tend to be overestimated. The main source of experimental errors is not the noise of the detection circuit, an approximately Gaussian process, but systematic errors and uncontrolled events that may occur during the mixing process. It is therefore difficult to provide statistically relevant estimates of the uncertainty of the parameters, as it could only be achieved through a large number of similar experiments.

An "effective" time lag t_0 was introduced as an adjustable parameter in order to account for the delayed onset of the enzymatic reaction following the introduction of the hyperpolarized glucose into the NMR tube containing the enzyme, bearing in mind that the mixing must be a turbulent process with an inhomogeneous distribution of the polarization within the NMR tube. The mixing process is likely to cause some degree of nonreproducibility in the early stage of the experiments. In these circumstances, it may not be sufficient to describe the time-dependence of signals by such global variables only, but one should consider local values of the glucose concentration and/or its polarization. This of course is mostly relevant for the early stages of the experiments. The effective time lag t_0 and the initial glucose concentration $[G]_0$ were therefore introduced *empirically* to represent the complex mixing process by a simple description. This partly empirical description of the glucose and G6P signals may explain the relatively wide ranges of fitted glucose concentrations and effective time lags t_0 in Table 1. These parameters may be correlated since they are ill-defined. Because of the limitations of the model, the resulting values should be interpreted with care.

The main objective of our study was to test the possibility of extracting kinetic parameters from our NMR experiments on a short time scale of about 20 s. Therefore, the determination of the catalytic constants k was our primary concern, and our analyses of the two anomeric signals provided the average values $k \sim 11.6 \times 10^3$ s^{-1} M^{-1} and $k \sim 18.4 \times 10^3$ s^{-1} M^{-1} for the α- and β-anomers, respectively. Note that the observation window of the enzymatic catalysis is much shorter than the characteristic time of the interconversion of the α to β anomers. The latter process therefore does not interfere with the determination of the rate constants of the phosphorylation reactions.

In conclusion, we have shown that D-DNP allows one to determine kinetic parameters of enzymatic reactions in less than 20 s, using a simple model that takes into account the inhibition by the reaction product. To our surprise, both α- and β-glucose anomers were found to be phosphorylated at similar rates. Beyond these findings, our study points to several improvements that could make the method more quantitative. Although clearly beyond the scope of this Letter, these include improvements of the mixing process, so as to obtain a more rapid homogenization of the reactants, as well as a more realistic description of the initial stage of the reaction. Additional improvements, such the use of selectively ^{13}C-labeled compounds or homonuclear $^{13}C-^{13}C$ spin decoupling, are currently under investigation.

EXPERIMENTAL METHODS

DNP. All DNP experiments reported herein were performed on a home-built DNP polarizer operating at T = 1.2 K in a static

dx.doi.org/10.1021/jz501411d | J. Phys. Chem. Lett. 2014, 5, 3290−3295

magnetic field B_0 = 6.7 T. The polarizer was modified from its original version[16−18] to accommodate an improved NMR double resonance circuit for ^{1}H and ^{13}C, resonating at 285.23 and 71.73 MHz, respectively.[19−21] The design of the DNP insert allows one to perform ^{1}H → ^{13}C cross-polarization (CP) during microwave irradiation. When using the free radical 4-hydroxy-2,2,6,6-tetramethylpiperidine-1-oxyl (TEMPOL) as a polarizing agent, CP-DNP can yield large polarizations in short times. The initial polarization $P_0(^{13}C)$ = 6.7% of glucose in the NMR tube was determined by comparison of the signal intensities immediately after dissolution with those in a spectrum acquired on the same sample in Boltzmann equilibrium after complete relaxation at 300 K.

Sample Preparation. A volume of 37.5 μL of a solution containing 7.5 M [$^{13}C_6$-d_7] D-glucose (Cortecnet) dissolved in 20% H_2O and 80% D_2O was added to 12.5 μL of a 200 mM TEMPOL solution. For each DNP experiment, the resulting mixture was frozen in liquid nitrogen to form 5 pellets of 10 μL each, visually inspected to discard opaque pellets that indicate the formation of ice crystals known to be deleterious for DNP, and then transferred into the cryostat of the DNP polarizer, initially at 4.2 K and later lowered to 1.2 K. After polarization, the pellets were rapidly heated up with hot water, and the hyperpolarized solution was transferred from the polarizer to the NMR spectrometer and injected into a buffer solution containing the reactants required for phosphorylation, i.e., [Mg^{2+}] = 100 mM, [ATP] = 250 mM, [HK] = 30 μM (400 units). The pH was adjusted to 7.5 by addition of 1 M NaOH. Hexokinase (mainly the PII isoform) from an overexpressing yeast strain of *Saccharomyces cerevisiae* was purchased from Sigma-Aldrich.

NMR Experiments. Free induction decays of ^{13}C were obtained at 11.75 T (500 MHz for protons) with deuterium decoupling, using 10° nutation angles and 1 s recycle delays. No field-frequency lock was used during the experiments.

Spectral Analysis. The free induction decays were processed using the NMRDraw software.[22] The spectra were zero-filled, but no apodization or line broadening was used in order to preserve the multiplet structures (see Figures 2 and 3).

Each component of the C^1 doublet arising from the large $^1J(C^1,C^2)$ coupling constants of the β-anomer had a 1:2:1 intensity pattern, due to the nearly degenerate coupling constants $^2J(C^1, C^3)$ = 4.5 Hz and $^3J(C^1, C^6)$ = 4.0 Hz. The resonances of the $^{13}C^1$ signals of the α-anomer appeared as a doublet-of-doublets with a 1:1:1:1 intensity pattern, due to the nondegenerate coupling constants $^2J(C^1, C^5)$ = 2.1 Hz and $^3J(C^1, C^6)$ = 3.4 Hz. Line shapes were fitted using a quasi-Newton method implemented in the *optim* Scilab function. The spectral analyses used homemade scripts using Scilab software.[23]

Determination of Kinetic Parameters. The extraction of the model parameters used a differential evolution algorithm that was implemented in Scilab.[23] Integration of the differential equations was based on a simple implicit Euler scheme. Differential evolution was designed to find the global minimum of a cost function. However, since there is no proof of convergence for this kind of algorithm, ca. 30 optimization runs were performed while varying various parameters of the algorithm (number of population members, minimization strategy, maximum number of iterations).[14] The parameters associated with the lowest value of the cost function were retained as the optimum model parameters.

AUTHOR INFORMATION

Corresponding Author

*E-mail: daniel.abergel@ens.fr.

Notes

The authors declare no competing financial interest.

ACKNOWLEDGMENTS

This work was supported by the Swiss National Science Foundation, the Ecole Polytechnique Fédérale de Lausanne (EPFL), the Swiss Commission for Technology and Innovation (CTI), Bruker BioSpin Switzerland AG, the French CNRS, and the European Research Council (ERC).

REFERENCES

(1) Abragam, A.; Goldman, M. Principles of Dynamic Nuclear-Polarization. *Rep. Prog. Phys.* **1978**, *41*, 395−467.

(2) Ardenkjaer-Larsen, J. H.; Fridlund, B.; Gram, A.; Hansson, G.; Hansson, L.; Lerche, M. H.; Servin, R.; Thaning, M.; Golman, K. Increase in Signal-to-Noise Ratio of > 10,000 Times in Liquid-State NMR. *Proc. Natl. Acad. Sci. U. S. A.* **2003**, *100*, 10158−10163.

(3) Hilty, C.; Bowen, S. Applications of Dynamic Nuclear Polarization to the Study of Reactions and Reagents in Organic and Biomolecular Chemistry. *Org. Biomol. Chem.* **2010**, *8*, 3361−3365.

(4) Bowen, S.; Sekar, G.; Hilty, C. Rapid Determination of Biosynthetic Pathways Using Fractional Isotope Enrichment and High-Resolution Dynamic Nuclear Polarization Enhanced NMR. *NMR Biomed.* **2011**, *24*, 1016−1022.

(5) Nelson, S. J.; Kurhanewicz, J.; Vigneron, D. B.; Larson, P. E. Z.; Harzstark, A. L.; Ferrone, M.; van Criekinge, M.; Chang, J. W.; Bok, R.; Park, I.; et al. Metabolic Imaging of Patients with Prostate Cancer Using Hyperpolarized [1-^{13}C] Pyruvate. *Sci. Transl. Med.* **2013**, *5*, 198ra108.

(6) Day, S. E.; Kettunen, M. I.; Gallagher, F. A.; Hu, D.-E. E.; Lerche, M.; Wolber, J.; Golman, K.; Ardenkjaer-Larsen, J. H. Brindle, K. M. Detecting Tumor Response to Treatment Using Hyperpolarized ^{13}C Magnetic Resonance Imaging and Spectroscopy. *Nat. Med.* **2007**, *13*, 1382−7.

(7) Lerche, M. H.; Meier, S.; Jensen, P. R.; Baumann, H.; Petersen, B. O.; Karlsson, M.; Duus, J. O.; Ardenkjær-Larsen, J. H. Study of Molecular Interactions with ^{13}C DNP-NMR. *J. Magn. Reson.* **2010**, *203*, 52−56.

(8) Bowen, S.; Hilty, C. Time-Resolved Dynamic Nuclear Polarization Enhanced NMR Spectroscopy. *Angew. Chem., Int. Ed.* **2008**, *47*, 5235−5237.

(9) Barb, A. W.; Hekmatyar, S. K.; Glushka, J. N.; Prestegard, J. H. Probing Alanine Transaminase Catalysis with Hyperpolarized ^{13}CD3-pyruvate. *J. Magn. Reson.* **2013**, *228*, 59−65.

(10) Harris, T.; Degani, H.; Frydman, L. Hyperpolarized ^{13}C NMR Studies of Glucose Metabolism in Living Breast Cancer Cell Cultures. *NMR Biomed.* **2013**, *26*, 1831−1843.

(11) Xu, Q.; Bush, C. A. Measurement of Long-Range Carbon-Carbon Coupling Constants in a Uniformly Enriched Complex Polysaccharide. *Carbohydr. Res.* **1998**, *306*, 335−339.

(12) Blume, A.; Fitzen, M.; Benie, A. J.; Peters, T. Specificity of Ligand Binding to Yeast Hexokinase PII Studied by STD-NMR. *Carbohydr. Res.* **2009**, *344*, 1567−1574.

(13) Mieville, M.; Jannin, J.; Helm, L.; Bodenhausen, G. Kinetics of Yttrium-Ligand Complexation Monitored Using Hyperpolarized ^{89}Y as a Model for Gadolinium in Contrast Agents. *J. Am. Chem. Soc.* **2010**, *132*, 5006−5007.

(14) Storn, R.; Price, K. Differential Evolution - A Simple and Efficient Heuristic for Global Optimization over Continuous Spaces. *J. Global Optim.* **1997**, *11*, 341−359.

(15) Dalvit, C.; Bodenhausen, G. Proton Chemical Shift Anisotropy: Detection of Cross-Correlation with Dipole−Dipole Interactions by Double-Quantum Filtered Two-Dimensional NMR Exchange Spectroscopy. *Chem. Phys. Lett.* **1989**, *161*, 554−560.

(16) Comment, A.; van den Brandt, B.; Uffmann, K.; Kurdzesau, F.; Jannin, S.; Konter, J. A.; Hautle, P.; Wenckebach, W. T. H.; Gruetter, R.; van der Klink, J. J. Design and Performance of a DNP Prepolarizer Coupled to a Rodent MRI Scanner. *Concepts Magn. Reson. B* **2007**, *31*, 255−269.
(17) Comment, A.; van den Brandt, B.; Uffmann, K.; Kurdzesau, F.; Jannin, S.; Konter, J. A.; Hautle, P.; Wenckebach, W. T. H.; Gruetter, R.; van der Klink, J. J. Principles of Operation of a DNP Prepolarizer Coupled to a Rodent MRI Scanner. *Appl. Magn. Reson.* **2008**, *34*, 313−319.
(18) Jannin, S.; Comment, A.; Kurdzesau, F.; Konter, J. A.; Hautle, P.; van den Brandt, B.; van der Klink, J. J. A 140 GHz Prepolarizer for Dissolution Dynamic Nuclear Polarization. *J. Chem. Phys.* **2008**, *128*, 241102.
(19) Bornet, A.; Melzi, R.; Jannin, S.; Bodenhausen, G. Cross Polarization for Dissolution Dynamic Nuclear Polarization Experiments at Readily Accessible Temperatures 1.2 < T < 4.2 K. *Appl. Magn. Reson.* **2012**, *43*, 107−117.
(20) Jannin, S.; Bornet, A.; Melzi, R.; Bodenhausen, G. High Field Dynamic Nuclear Polarization at 6.7 T: Carbon-13 Polarization above 70% within 20 min. *Chem. Phys. Lett.* **2012**, *549*, 99−102.
(21) Bornet, A.; Melzi, R.; Perez Linde, A. J.; Hautle, P.; van den Brandt, B.; Jannin, S.; Bodenhausen, G. Boosting Dissolution Dynamic Nuclear Polarization by Cross Polarization. *J. Phys. Chem. Lett.* **2013**, *4*, 111−114.
(22) Delaglio, F.; Grzesiek, S.; Vuister, G. W.; Zhu, G.; Pfeifer, J.; Bax, A. NMRPipe: A Multidimensional Spectral Processing System Based on UNIX Pipes. *J. Biomol. NMR* **1995**, *6*, 277−293.
(23) *Scilab*; version 5.5; Free and Open Source Software for Numerical Computation; Scilab Consortium, Digiteo: Paris, 2011.